Materials Science & Engineering C 131 (2021) 112525

Contents lists available at ScienceDirect

Materials Science & Engineering C

journal homepage: www.elsevier.com/locate/msec

3D-printed alginate-hydroxyapatite aerogel scaffolds for bone tissue engineering

Ana Iglesias-Mejuto, Carlos A. García-González *

Department of Pharmacology, Pharmacy and Pharmaceutical Technology, I+D Farma group (GI-1645), Faculty of Pharmacy and Health Research Institute of Santiago de Compostela (IDIS), Universidade de Santiago de Compostela, E-15782 Santiago de Compostela, Spain

ARTICLE INFO

Keywords:
3D-printing
Supercritical drying
Aerogel
Bone scaffold
Hydroxyapatite

ABSTRACT

3D-printing technology allows the automated and reproducible manufacturing of functional structures for tissue engineering with customized geometries and compositions by depositing materials layer-by-layer with high precision. For these purposes, the production of bioactive gel-based 3D-scaffolds made of biocompatible materials with well-defined internal structure comprising a dual (mesoporous and macroporous) and highly interconnected porosity is essential. In this work, aerogel scaffolds for bone regeneration purposes were obtained by an innovative strategy that combines the 3D-printing of alginate-hydroxyapatite (HA) hydrogels and the supercritical CO_2 drying of the gels. BET and SEM analyses were performed to assess the textural parameters of the obtained aerogel scaffolds and the dimensional accuracy to the original computer-aided design (CAD) design was also evaluated. The biological characterization of the aerogel scaffolds was also carried out regarding cell viability, adhesion and migration capacity. The obtained alginate-HA aerogel scaffolds were highly porous, biocompatible, with high fidelity to the CAD-pattern and also allowed the attachment and proliferation of mesenchymal stem cells (MSCs). An enhancement of the fibroblast migration toward the damaged area was observed in the presence of the aerogel formulations tested, which is positive in terms of bone regeneration.

1. Introduction

Bone defects resulting from tumors, infections, trauma, biochemical disorders and abnormal skeletal developments generate severe health problems and represent high sociosanitary costs for the national health services [1]. Biological grafts (autografts, allografts) and non-degradable grafts (metallic and ceramic implants) are the most common solutions for these pathologies. However, their low availability (for biological grafts) and frequent post-surgical complications such as the lack of osseointegration or the generation of immune response (for non-degradable grafts) are among the important drawbacks that may occur [2]. Regenerative medicine aims to anatomically and functionally restore damaged tissues using a combination of (i) advanced biodegradable 3D-scaffolds as temporary extracellular matrices (ECM), (ii) cells, and (iii) growth factors [2,3]. The processing method used to obtain these bone scaffolds should provide an optimum design to promote the new tissue formation. These bone scaffolds should have a well-defined internal structure, dual interconnected porosity and bioactivity. Given the increasing complexity in morphology and composition of these structures and the high sensitivity to processing environments (*e.g.*, high temperature, shear stress, pH, use of organic solvents), innovative and benign strategies are sought to generate these new biomedical products [4].

3D-printing is a cutting-edge technology that allows the automated and reproducible fabrication of functional, scalable and customized artificial structures for personalized medicine [5]. In general, this technology uses a layer-by-layer deposition of biocompatible materials to achieve stable 3D-constructs. Specifically, extrusion-based bioprinting is an additive manufacturing technique commonly used to create hydrogel scaffolds [6,7]. It is a pressure-based method that employs a robotic system linked to a bioink dispensing syringe. A computer-aided design (CAD) is used to deposit the bioink in a 3D-predefined shaped structure. This technique is able to print different tissues with the generation of anatomically correct macroporous structures [8]. A limited (but growing) number of biomaterials are suitable for bioink formulations to generate 3D-printed scaffolds as they must be printable, biocompatible and present attractive structural and mechanical properties [9]. Nevertheless, structures obtained by 3D-printing have the customized external morphology essential for personalized medicine, but they usually lack the high precision required to generate

* Corresponding author.
E-mail address: carlos.garcia@usc.es (C.A. García-González).

https://doi.org/10.1016/j.msec.2021.112525
Received 30 July 2021; Received in revised form 18 October 2021; Accepted 23 October 2021
Available online 27 October 2021

nanostructured scaffolds, with a control in the macro and microstructural levels. For this reason, the combination of 3D-printing with other techniques is needed to yield customized nanostructured biomaterials.

Polymeric nanostructures with advanced properties can be obtained using supercritical fluid technology based on the use of supercritical carbon dioxide ($scCO_2$) [10]. Namely, $scCO_2$-assisted drying is adequate for the extraction of the solvent of a gel while preserving the internal gel structural properties, such as high porosity and high specific surface areas, in the so-called aerogels. This technology can be used to obtain aerogel-containing grafts and implants [11], among them aerogel bone scaffolds for tissue engineering applications [12–14]. Aerogels present a high mesoporosity comparable to that of the native ECM, which favor cell growth, and can be obtained from polysaccharides and proteins [15].

Alginate is a natural biopolymer widely used for bone scaffolds and for bioink formulation because it is biocompatible, biodegradable, non-toxic and non-immunogenic, and supports cell growth [16]. Alginate generates a stable hydrogel in the presence of low concentrations of divalent cations, namely Ca^{2+} which presents the advantage of its low toxicity with respect to other divalent ions. Finally, alginate composition resembles glycosaminoglycan (GAG) structure, one of the major components of the natural ECM in human tissue. However, alginate-based structures usually lack bioactivity and should be combined with other admixtures for bone tissue engineering purposes [17].

Hydroxyapatite (HA) is the major inorganic component in mammalian hard tissues and also an excellent bone substitute material because it is bioactive, osteoconductive, non-toxic and highly biocompatible due to its chemical and structural similarity to natural bone minerals [18,19]. This chemical similarity is essential for apatite deposition and subsequent bone regeneration. HA may also have a role as a cross-linking agent and as an inorganic mechanical reinforcer [20]. Moreover, HA and its composites are suitable for attachment, proliferation and differentiation of mesenchymal stem cells (MSCs). All these properties render HA favorable for osteointegration [21–23]. The source and size of HA particles is an important factor on alginate-HA gel scaffolds, because the HA grain size and specific surface area affect the gelling time and rheological properties of the hydrogels. MicroHA has been proposed for applications requiring rapid gelation kinetics and improved mechanical properties, while nanoHA is appropriate to render homogeneous hydrogels under more controlled gelation kinetics [20]. Overall, alginate-HA composites are promising candidates for bone tissue engineering where HA also triggers the mineralization process and stimulates calcium phosphate and HA nanocrystals nucleation and growth [19,21].

Strategies for the generation of a complex 3D-shaped structures with different functionalities and architectures ranging from the nanoscale to the macroscale are under development to generate structures with this pore hierarchy [24]. The design and optimization of the final pore structure (pore size hierarchy and proportions) is also essential for the material performance in tissue engineering applications. The use of aerogel technology can solve some of the current 3D-printing limitations regarding the nanostructuration of 3D-scaffolds, but the production of aerogels with a customized external morphology is a remaining remarkable challenge [25]. Recently, several 3D-printed aerogels have shown an excellent printability in the wet state and the preservation of their textural properties like a high specific surface area [25–27]. Nevertheless, aerogels usually lack macroporosity and methods to confer it and to control the macropore size are under development [28,53–55]. In general, aerogels with various pore size ranges are highly desirable for applications like bone tissue engineering [29].

The unexplored combination of 3D-printing and aerogel technologies for bone tissue engineering is herein proposed as a win-win strategy to obtain biomaterials with improved performance and architecture. Finally, new strategies to improve the aerogels strengthening and the printing process necessary to obtain more fine and intricate structures are still a challenge nowadays. In this work, 3D-printed alginate aerogel scaffolds containing hydroxyapatite were processed by a combination of 3D-printing of hydrogels and supercritical CO_2 drying for bone regeneration purposes. The effects of alginate, HA and Ca^{2+} concentrations on the 3D-printed hydrogel scaffolds processability were assessed. Then, the 3D-printed aerogels obtained after supercritical drying were evaluated regarding their textural (specific surface area, porosity, density, shrinkage) and biological (cyto- and hemocompatibility, adhesion, migration) properties. The fidelity of the different gel formulations with respect to the original CAD file was also evaluated.

2. Materials and methods

2.1. Materials

Alginic acid sodium salt from brown algae with medium viscosity (guluronic acid/mannuronic acid ratio of 70/30, Mw 403 kDa, 3170 cps) and calcium chloride ($CaCl_2$; M_w 110.98 g/mol, 99.99% purity) were provided by Sigma Aldrich (Madrid, Spain). Hydroxyapatite (HA; M_w 502.31 g/mol, reagent grade purity, micropowder) was provided by Fluidinova (Moreira da Maia, Portugal). CO_2 (purity >99.9%) was supplied by Nippon Gases (Madrid, Spain) and absolute ethanol (EtOH) by VWR (Radnor, PA, USA). Water was purified using reverse osmosis (resistivity >18 MΩ·cm; Milli-Q, Millipore®, Madrid, Spain).

2.2. 3D-printing of hydrogel scaffolds

Aqueous bioinks with three different alginate concentrations (6, 8 and 10 wt% with respect to water) were prepared using milliQ water as a solvent. Furthermore, different HA concentrations (0, 8, 16 and 24 wt% with respect to water) were added to the 6 wt% alginate solutions. All alginate solutions were prepared under vigorous agitation (600 rpm) employing a homogenizer (VWR vos 60, Pennsylvania, USA) for at least 1 h at room temperature (RT). The thus obtained alginate solutions were degassed in a sonication bath (Branson 3510 Emerson, Ferguson, MO, USA) for 10 min to eliminate air bubbles. Hydrogels were obtained by printing the alginate inks with a Cellink BIOX Bioprinter (Boston, MA, USA) at RT using an extrusion printhead with a 3-mL syringe and a 410-μm nozzle at the printing pressure of 50 kPa and a printing velocity of 12 mm/s. 3D-printed alginate hydrogels with dimensions of 20x20x1 mm (for physicochemical tests, *cf.* Sections 2.4 and 2.5) and 10x10x1 mm (for biological tests, *cf.* Sections 2.6 to 2.8) were obtained using a grid pattern and 3 layers. After the printing process, all scaffolds were put directly in contact with $CaCl_2$ aqueous solutions (0.1, 0.5 and 1 M) for gelation (Fig. S1 of Supplementary Info).

2.3. Supercritical drying of 3D-printed gels

Alginate hydrogels turn alcogels by immersion in absolute EtOH. Two solvent exchanges to ethanol were carried out with an exchange frequency of 24 h. The alcogels were wrapped in filter paper and dried by supercritical drying to obtain the aerogels. Briefly, gels were placed into a 100-mL stainless steel autoclave (Thar Process, Pittsburg, PA, USA) and immersed in 25 mL of absolute ethanol to prevent them from shrinkage before being in contact with compressed CO_2. $scCO_2$ was supplied using a dual piston pump and introduced from the top of a vessel heated at the constant temperature of 40 °C. Firstly, a continuous CO_2 flow rate (5–7 g/min) at 120 bar took place for 4 h. Aerogels were then obtained after CO_2 depressurization at a rate of 2 bar/min, collected from the autoclave and stored for characterization. The obtained scaffolds were denoted as Alg *x*%,HA *y*%,$CaCl_2$ *z*M (x = 6, 8, 10 wt%; y = 8, 16, 24 wt%; z = 0.1, 0.5, 1 M).

2.4. Physicochemical characterization of alginate aerogel scaffolds

The skeletal density of the aerogels (ρ_{skel}) was determined using a helium pycnometer (Quantachrome, Boynton Beach, FL, USA) at 25 °C

and 1.01 bar. Values were obtained from five replicates. The apparent density of the aerogel scaffolds formulations (ρ_{app}) was determined following the Eq. (1):

$$\rho_{app} = \text{Aerogel mass}/\text{Aerogel volume} \quad (1)$$

where the volume of the aerogels was obtained by measuring the three dimensions of the aerogel obtained with a digital caliper (Fowler™, Newton, MA, USA). The porosity of the structures (ε) was obtained from Eq. (2) from the specific volume considering the external dimensions of the material (V_t) and the specific volume occupied by the voids in the full volume ($V_{void,t}$).

$$\varepsilon = \left(1 - \left(\rho_{app}/\rho_{skel}\right)\right) \times 100 = \left(V_{void,t}/V_t\right) \times 100 \quad (2)$$

The inner porosity of the aerogel fibers (ε_f) was obtained from Eq. (3) from the specific volume occupied by the fibers (V_{fibers}) and the specific volume occupied by the voids (*i.e.* pores) in the fibers ($V_{void,fibers}$).

$$\varepsilon_f = \left(V_{void,fibers}/V_{fibers}\right) \times 100 \quad (3)$$

$$V_{void,fibers} = V_{fibers} - (1/\rho_{skel}) \quad (4)$$

The volumetric shrinkage (in percentage) of the aerogel scaffolds was calculated from the external dimensions of the material before and after supercritical drying following the Eq. (5):

$$\text{Volume shrinkage} = [(\text{Alcogel volume}–\text{Aerogel volume})/\text{Alcogel volume}] \times 100 \quad (5)$$

Low-temperature N_2 adsorption/desorption analysis (ASAP 2000 Micromeritics Inc.; Norcross, GA, USA) was performed to assess aerogel textural properties. Before measurements, samples were degassed under vacuum at 40 °C for 24 h. Specific surface area (A_{BET}) of aerogels was evaluated employing the BET (Brunauer–Emmett–Teller) method. Specific pore volume (V_p), pore size distributions and mean pore diameter (d_p) were determined applying the BJH (Barrett–Joyner–Halenda) method. The morphology of the aerogels was evaluated by scanning electron microscopy (SEM, EVO LS15, Zeiss, Oberkochen, Germany). Aerogel samples were iridium-sputtered prior to imaging to minimize charging and to improve the image quality.

2.5. Dimensional accuracy tests

Two indices (printing accuracy and shape fidelity factor –SFF–) were employed to assess the fidelity of the gel structures (for alcogels and aerogels) with respect to the original printing file processed by 3D-printing in the first step of the dual processing strategy herein proposed. The printing accuracy and SFF were calculated from Eqs. (6) and (7), respectively:

$$\text{Printing accuracy } (\%) = [1 - ((|AA–\text{Ail})/\text{Ai})] \times 100 \quad (6)$$

$$\text{SFF} = \text{Ai}/\text{A} \quad (7)$$

where A_i is the alcogel or aerogel printed area respectively, and A is the CAD area (printing file).

2.6. Cell viability tests

The cytocompatibility of the different alginate-HA aerogel scaffolds was determined by assessing the viability of mouse embryo fibroblasts (BALB/c3 T3) after 24 and 48 h of culture in the presence of the aerogel formulations using the WST-1 test and in triplicate. This test is based on the degradation of WST-1 into formazan and is directly correlated with the number of metabolically active cells. BALB cells (6500 cells/cm^2) were seeded in 24-well plates in DMEM supplemented with 15% fetal bovine serum, penicillin 100 U/mL and streptomycin 100 g/mL. Cells were incubated at 37 °C in a humidified atmosphere enriched with 5% CO_2. Scaffolds (1 × 1 × 0.1 cm) were UV-sterilized for 1 h and then placed in the wells with cells containing 1500 μL of DMEM supplement. Positive controls of cells with 1000 μL of medium and blanks of 1000 μL of medium (both in triplicate) were maintained at the same conditions. After 24 and 48 h of culture, scaffolds were removed, 250 μL of medium was left in the wells and 25 μL of WST 1 reagent was added. The plate was incubated for 2 h at the same conditions and then shaken thoroughly for 1 min. Finally, 110 μL were transferred to a 96-well plate to measure the absorbance at λ = 450 nm in a microplate reader (Infinite® M200, Tecan Group Ltd., Männedorf, Switzerland).

2.7. Cell attachment tests

The spreading of human bone marrow mesenchymal stem cells (MSCs) onto the scaffolds was evaluated by DAPI staining to visualize the cellular nuclei after 6 and 13 days of culture [30]. MSC-seeded scaffolds were fixed with paraformaldehyde (4% wt/v) for 10 min and washed with PBS. Then, they were incubated in Triton/PBS (0.2% *v*/v) solution for 5 min. Finally, scaffolds were washed with PBS, placed on glass slides, and one drop of the DAPI-containing ProLong gold antifade mountant (Molecular Probes Inc., Eugene, OR, USA) was added to each scaffold before their storage at −20 °C. Finally, cell attachment in the scaffolds was evaluated using a Leica TCS-SP2 spectral confocal microscope (Leica TCS-SP2, Leica Microsystems Heidelberg GmbH, Mannheim, Germany) [31]. An open source software (ImageJ 1.5i, US National Institutes of Health, Bethesda, MD, USA) was used to analyze the captured images.

2.8. Migration assay

Cell migration was evaluated by a scratch wound healing assay [32,33]. After the confluence, BALB cells monolayer was scratched by a straight line using a sterile pipette tip and mimicking a wound *in vitro*. PBS was then employed to wash cells and remove cell debris. The different aerogel scaffold formulations were placed in the wells with fresh cell culture medium at 37 °C. Photographs of the scratch wound were obtained with an inverted microscope (Olympus, Japan) immediately (t = 0 h) and at 24 h to analyze the cell migration. The migration area (%) was assessed as follows (Eq. (8)):

$$\text{Migration area } (\%) = (A_0–A_n)/A_0 \times 100 \quad (8)$$

where A_0 represents the initial wound area (t = 0 h) and A_n represents the residual wound area at 24 h measured by ImageJ software.

2.9. Statistical analysis

Results of cell viability tests for each aerogel scaffold type (n = 3) were reported as mean value ± standard deviation. t-tests were carried out to determine the statistical significance of the differences among the groups, and values of $p < 0.05$ were considered as statistically significant.

3. Results and discussion

3.1. Effect of alginate and $CaCl_2$ concentration on scaffolds

The feasible operating region of alginate ink formulation composition and Ca^{2+} concentration ranges for 3D-printing was firstly determined. The following criteria were followed: (i) alginate bioink must be liquid-like in the printhead to avoid the tip clogging, but (ii) it must be solid-like in the printbed to maintain the customized 3D-geometry during the deposition process and avoid the structural integrity loss.

Homogeneous 3D-structures formed by differentiated filaments arranged in layers were accordingly obtained with alginate concentrations in the 6–10 wt% range and a $CaCl_2$ concentration of 0.5 M (Fig. 1). Inks

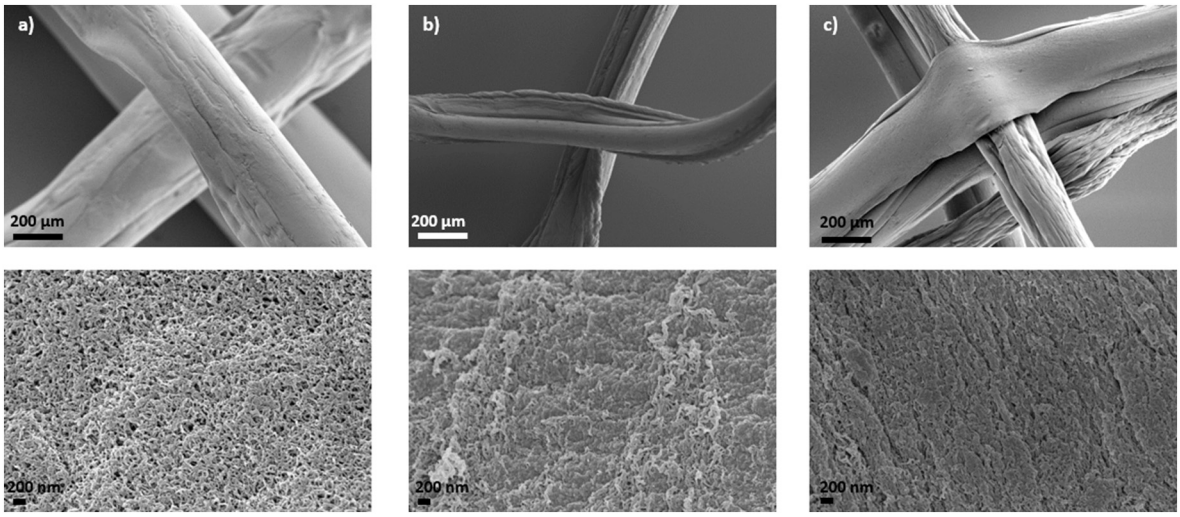

Fig. 1. SEM pictures of 3D-printed alginate aerogels prepared at $CaCl_2$ concentration of 0.5 M and from aqueous alginate inks of different concentrations: a) 6, b) 8, and c) 10 wt%. Aerogels are observed at two different magnifications.

below or above this alginate concentration range were discarded due to the non-homogeneous appearance obtained for the 3D-printed hydrogels. The 3D-structure and porosity, with mesopores and macropores, was clearly recognized in all aerogels produced in the feasible region. Tighter fiber interactions appear to be present at alginate concentrations of 10 wt%. A highly interconnected structure with mesopores and macropores was observed. An improvement in the textural parameters (A_{BET} and V_p) in all aerogels was also observed (Table 1) with respect to other alginate aerogels previously described [34].

Ionic crosslinking of alginate gels provided long-term stability to final structures in the 0.1–1 M $CaCl_2$ range. Alginate scaffolds crosslinked at this $CaCl_2$ concentration range had a highly porous structure throughout the scaffold with a high aerogel surface area (Fig. 2 and Table 1). Finally, alginate scaffolds crosslinked with $CaCl_2$ 1 M solution had more homogeneously printed strands, which could be attributed to more Ca^{+2} ions being involved in the ionic crosslinking of the alginate [35]. In general, aerogel scaffolds obtained at alginate concentration 6 wt% and gelified with $CaCl_2$ 1 M exhibited non-woven fibers with tighter junctions if compared to the rest of formulations studied and resulting in less brittle constructs.

High values of textural properties were obtained for all the tested aerogel formulations, although the composition and crosslinker concentration had an influence in the results (Table 1), being the highest values found in aerogels obtained from inks using an alginate concentration of 6 wt% (Table 1). A similar trend in terms of textural properties was obtained in aerogels from alginate and alginate composites, like alginate-pectin microspheres generated with different alginate-to-pectin proportions [36].

Table 1
Textural properties of aerogel-based scaffolds from inks at different alginate (6, 8, 10 wt%) concentrations and crosslinked in gelation baths of different $CaCl_2$ (0.1, 0.5, 1 M) concentrations. Notation: A_{BET}: specific BET surface area, d_p: BJH-mean pore diameter, V_p: BJH-specific pore volume.

Aerogel scaffold	A_{BET} (m^2/g)	d_p (nm)	V_p (cm^3/g)
Alg 6%, HA 0%, $CaCl_2$ 0.1 M	438 ± 22	22 ± 1	3.14 ± 0.16
Alg 6%, HA 0%, $CaCl_2$ 0.5 M	277 ± 14	22 ± 1	2.00 ± 0.10
Alg 6%, HA 0%, $CaCl_2$ 1 M	183 ± 9	19 ± 1	1.16 ± 0.06
Alg 8%, HA 0%, $CaCl_2$ 0.1 M	180 ± 9	17 ± 1	0.95 ± 0.05
Alg 8%, HA 0%, $CaCl_2$ 0.5 M	177 ± 9	22 ± 1	1.00 ± 0.05
Alg 8%, HA 0%, $CaCl_2$ 1 M	147 ± 7	21 ± 1	0.97 ± 0.05
Alg 10%, HA 0%, $CaCl_2$ 0.1 M	172 ± 9	18 ± 1	1.04 ± 0.05
Alg 10%, HA 0%, $CaCl_2$ 0.5 M	158 ± 8	16 ± 1	0.87 ± 0.04
Alg 10%, HA 0%, $CaCl_2$ 1 M	219 ± 11	14 ± 1	1.11 ± 0.06

3.2. Effect of hydroxyapatite concentration on scaffold morphology

Alginate hydrogel printing resulted in stable single filaments (Fig. 1), but without significant binding between layers. Moreover, alginate aerogel scaffolds started to dissolve just after their immersion in aqueous solutions losing their integrity after 24 h. The addition of HA to the alginate ink was hypothesized to preserve the strands geometry while improving structure stability and bioactivity of scaffolds yielding an improved 3D-structure for bone tissue engineering. HA is hydrophobic and the scaffolds would dissolve more gradually under physiological conditions and maintain their shape, at the expense of a reduction in the porosity of the structure [37,38]. To compensate this, alginate aerogels were herein crosslinked at high concentrations of the divalent cations solution ($CaCl_2$ 1 M), so that more cations were captured inside the scaffolds and bridged the gel network. Finally, HA is involved in protein adsorption and this process causes cells transportation into the scaffold, which is positive because it may promote cell adhesion and proliferation on scaffold surfaces [39].

Homogeneous 3D-structures were obtained for the HA concentration range tested (0–24 wt%) with fibers and layers consistently arranged. The macroporous and mesoporous structures of the scaffolds were maintained as well. At higher HA concentrations, more HA granules appear forming the filaments stacked together with the alginate (Fig. 3). The easy handling of the synthesized alginate-HA scaffolds and the SEM images showing binding between strands appear to confirm the structural integrity and stability of the aerogels after 3D-printing.

N_2 adsorption-desorption analysis of alginate-HA aerogel scaffolds show an important decrease in the specific surface area and total pore volume, while the pore diameter is almost unaltered with respect to scaffolds fabricated with alginate only (Table 2). The decrease in the total pore volume could be attributed to the interactions between $–NH_3^+$ groups of alginate and –OH groups and Ca^{2+} ions of HA that lead to the final deposition of HA over the scaffold creating an irregular surface structure [16]. In general, the HA addition decreased the textural properties in all alginate-HA formulations, due to the low mesoporosity of the HA powder (2 m^2/g). Despite that, the textural properties of the HA-containing alginate aerogels may still be enough to favor cell seeding and nutrient diffusion throughout the scaffold structure. The results obtained in terms of textural parameters after the addition of HA are coherent with previous studies using other polymeric scaffolds [16,40]. Apparent density values increased gradually with the addition of HA resulting in a reverse effect on porosity, although all aerogel scaffold formulations tested reached values above 80% (Table 2). The porosity of

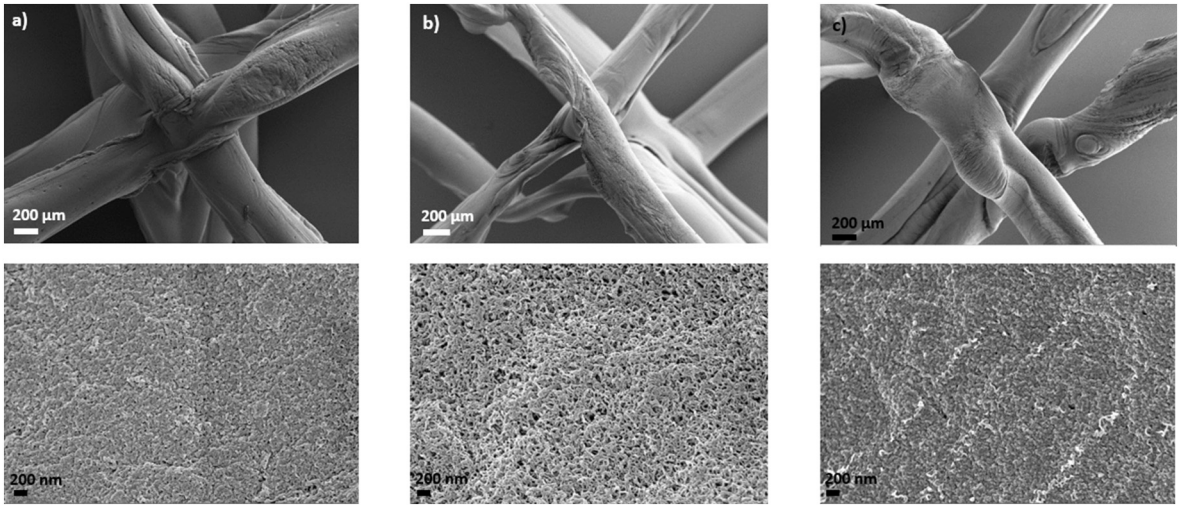

Fig. 2. SEM pictures of 3D-printed alginate aerogels prepared from 6 wt% aqueous alginate inks and at different $CaCl_2$ concentrations: a) 0.1, b) 0.5 and c) 1 M. Aerogels are observed at two different magnifications.

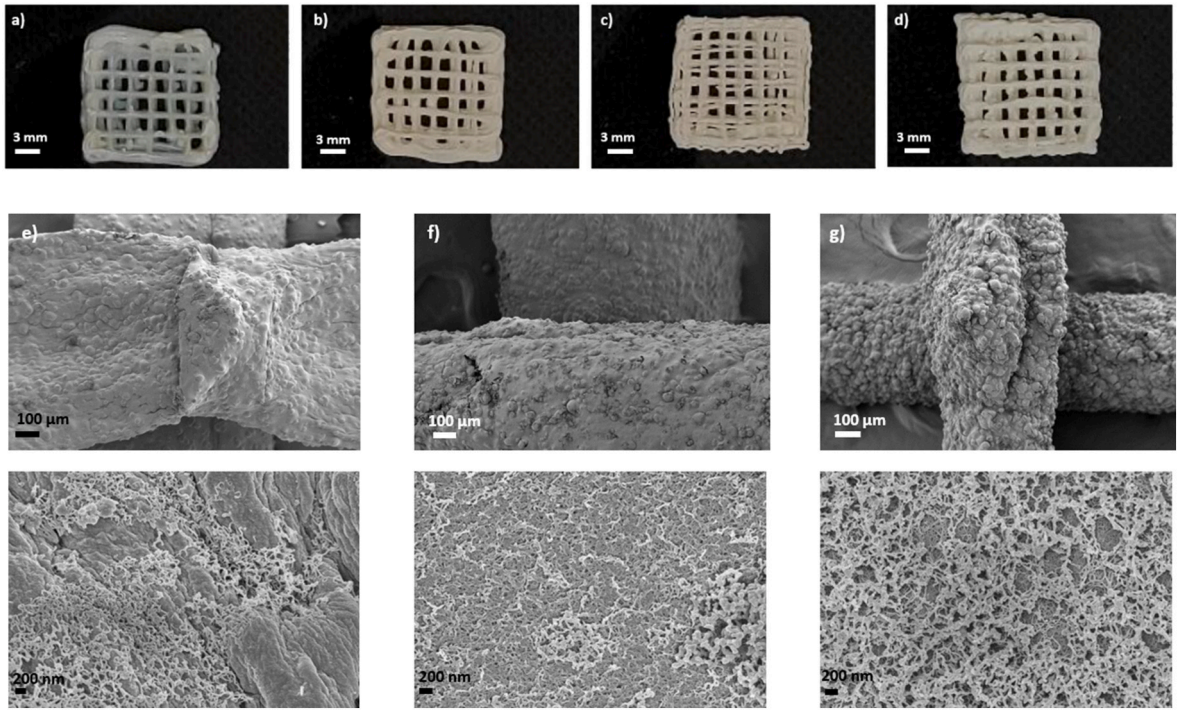

Fig. 3. Images and SEM pictures of 3D-printed alginate-HA aerogels prepared from 6 wt% alginate inks with different HA concentrations: (a) 0, (b, e) 8, (c, f) 16, and (d, g) 24 wt%. In all cases the gelation was performed using 1 M $CaCl_2$ solutions. Aerogesl are observed at two different magnifications.

Table 2
Textural properties of aerogel-based scaffolds processed from 6 wt% alginate inks with different HA concentrations (0, 8, 16, 24 wt%) and crosslinked with $CaCl_2$ 1 M solution. Notation: A_{BET}: specific BET surface area, d_p: BJH-mean pore diameter, V_p: BJH-specific pore volume, ρ_{app}: *apparent density,* ρ_{skel}: skeletal density, ε*: scaffold porosity,* ε_f*: aerogel fibers porosity*.

Aerogel scaffold	A_{BET} (m^2/g)	d_p (*nm*)	V_p (cm^3/g)	ρ_{app} (*g/ mL*)	ρ_{skel} (*g/ cm*^{3})	ε (*%*)	ε_f (*%*)
Alg 6%, HA 0%, $CaCl_2$ 1 M	183 ± 9	19 ± 1	1.16 ± 0.06	0.14 ± 0.01	1.18 ± 0.16	88.56 ± 1.29	86.58 ± 2.26
Alg 6%, HA 8%, $CaCl_2$ 1 M	118 ± 6	24 ± 1	0.99 ± 0.05	0.24 ± 0.03	1.72 ± 0.09	85.85 ± 1.59	85.25 ± 4.02
Alg 6%, HA 16%, $CaCl_2$ 1 M	67 ± 3	26 ± 1	0.60 ± 0.03	0.29 ± 0.04	1.93 ± 0.04	85.06 ± 2.40	79.78 ± 3.92
Alg 6%, HA 24%, $CaCl_2$ 1 M	29 ± 2	31 ± 2	0.21 ± 0.01	0.34 ± 0.02	1.72 ± 0.14	80.33 ± 1.19	76.68 ± 3.54

the fibers also decreased with the addition of HA. The total porosity values of the scaffolds (88.56 to 80.33%) are slightly higher than the aerogel fibers porosity values (86.58 to 76.68%) as the scaffolds are formed by a 3D-mesh of vertically and horizontally aligned aerogel microfibers separated by macroporous gaps. These are good results since the addition of HA have strongly affected other textural parameters (A_{BET}) but not porosity. Nevertheless, higher porosity (80–99%) and lower densities (0.02 g/ cm^3 as bulk density) values were previously reported for alginate aerogel in the form of microparticles [41–43]. Consistently, the incorporation of HA has advantages (bioactivity, similarity to human bone mineral phase) [18,19] at the expense of a slight decrease in textural parameters.

The volumetric shrinkage of aerogel scaffolds after performing the supercritical drying was tested (Fig. 4) to unveil the influence of this process in the end aerogel scaffolds. The direct solvent exchange to ethanol resulted in aerogels without high volumetric shrinkage values and with reduced overall processing time. Structures containing HA had a lower volume shrinkage with respect to the formulation without HA (Alg 6%, HA 0%, $CaCl_2$ 1 M). These are good results since higher volume shrinkage values (42–65%) have been reported for alginate aerogels obtained by sequential solvent exchanges [44].

3.3. Dimensional accuracy tests

Printing accuracy and SFF indices were employed to assess the reproducibility and the fidelity of the dual processing strategy herein proposed. The values obtained for both parameters are higher when assessed in the alcogels than when assessed in the aerogels (Table 3). This feature was expected since the volume shrinkage reported in Section 3.2 influences the dimensional accuracy indices. Nonetheless, the alcogel printing accuracy and SFF values obtained are close to the values previously reported for 3D-printed alginate gels and for other polysaccharide gels [37,45].

3.4. Biocompatibility tests for aerogel scaffolds

BALB cells were cultured in the presence of alginate-HA aerogel scaffolds for cell cytotoxicity evaluation. Fig. 5 represents the cell viability after culture for 24 and 48 h with values reaching *ca.* 100% for alginate aerogels, which means that they had no negative effect on cell proliferation. Similar results on BALB cells viability after 48 h were found for alginate-HA aerogels, regardless of the HA concentration.

In general, these viability results indicate that neither the scaffold composition nor the dual processing strategy compromised the cell viability. The high cell viability observed after the tests confirmed the non-toxicity of the aerogel structures and correlates with scaffolds containing the same components [46]. Indeed, the biocompatibility of the initial components of the scaffolds (alginate and HA) was already reported [47]. Overall, these are promising results since cytocompatibility and a suitable microstructure (pore size and porosity) govern the properties of an ideal scaffold.

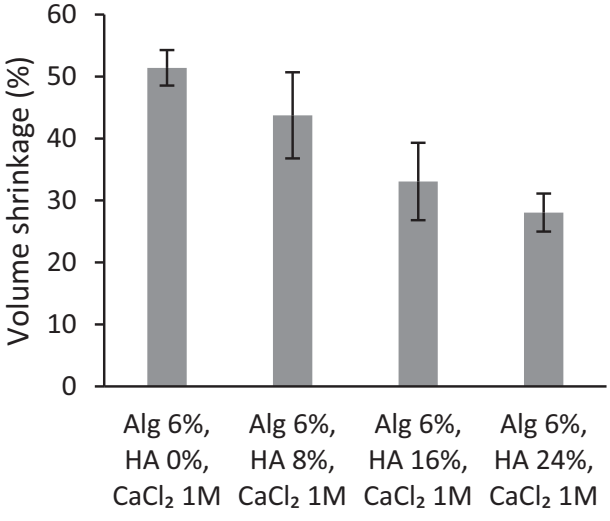

Fig. 4. Volume shrinkage (in percentage) of different alginate-HA formulations.

Table 3
Printing fidelity indices of aerogels prepared from alginate-HA formulations. Aerogels were manufactured at an alginate concentration of 6 wt%, at different HA concentrations (0, 8, 16 and 24 wt%) and at a $CaCl_2$ concentration of 1 M.

Aerogel scaffold	Alcogel Printing Accuracy (%)	Aerogel Printing Accuracy (%)	Alcogel SFF	Aerogel SFF
Alg 6%, HA 0%, $CaCl_2$ 1 M	77.73 ± 11.03	43.56 ± 12.94	0.82 ± 0.08	0.64 ± 0.05
Alg 6%, HA 8%, $CaCl_2$ 1 M	75.51 ± 8.54	39.06 ± 10.70	0.81 ± 0.05	0.62 ± 0.04
Alg 6%, HA 16%, $CaCl_2$ 1 M	83.51 ± 2.29	50.18 ± 6.05	0.86 ± 0.02	0.67 ± 0.03
Alg 6%, HA 24%, $CaCl_2$ 1 M	83.35 ± 6.21	48.14 ± 4.84	0.86 ± 0.05	0.66 ± 0.02

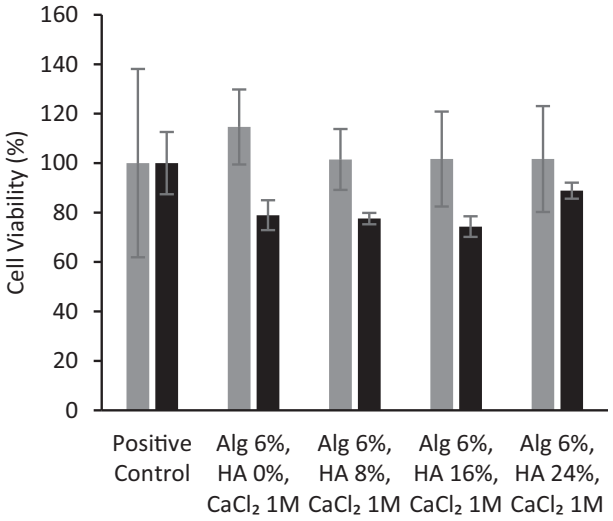

Fig. 5. Cell viability tests of alginate-HA aerogels. Viability (expressed in %) of BALB cells after 24 (grey bars) and 48 h (black) of contact with scaffolds determined by the WST-1 test. There was no statistically significant differences among groups (*t*-test; $p < 0.05$).

3.5. Cell attachment and proliferation tests on aerogel scaffolds

A challenge in tissue engineering is the generation of biomaterials with an adequate structure to act as a substrate for cell bonding, multiplication, development and reproduction [48]. MSCs attachment and proliferation in aerogels were herein tested as this cell line is attractive for tissue engineering applications aiming at the generation of artificial bone substitutes. MSCs present self-renewal potential, they can differentiate *in vivo* and *ex vivo* into different cell types like chondrocytes or osteoblasts and their isolation is not related to donor-site morbidity [49]. In the case of osteoblasts, their attachment to scaffolds depends on

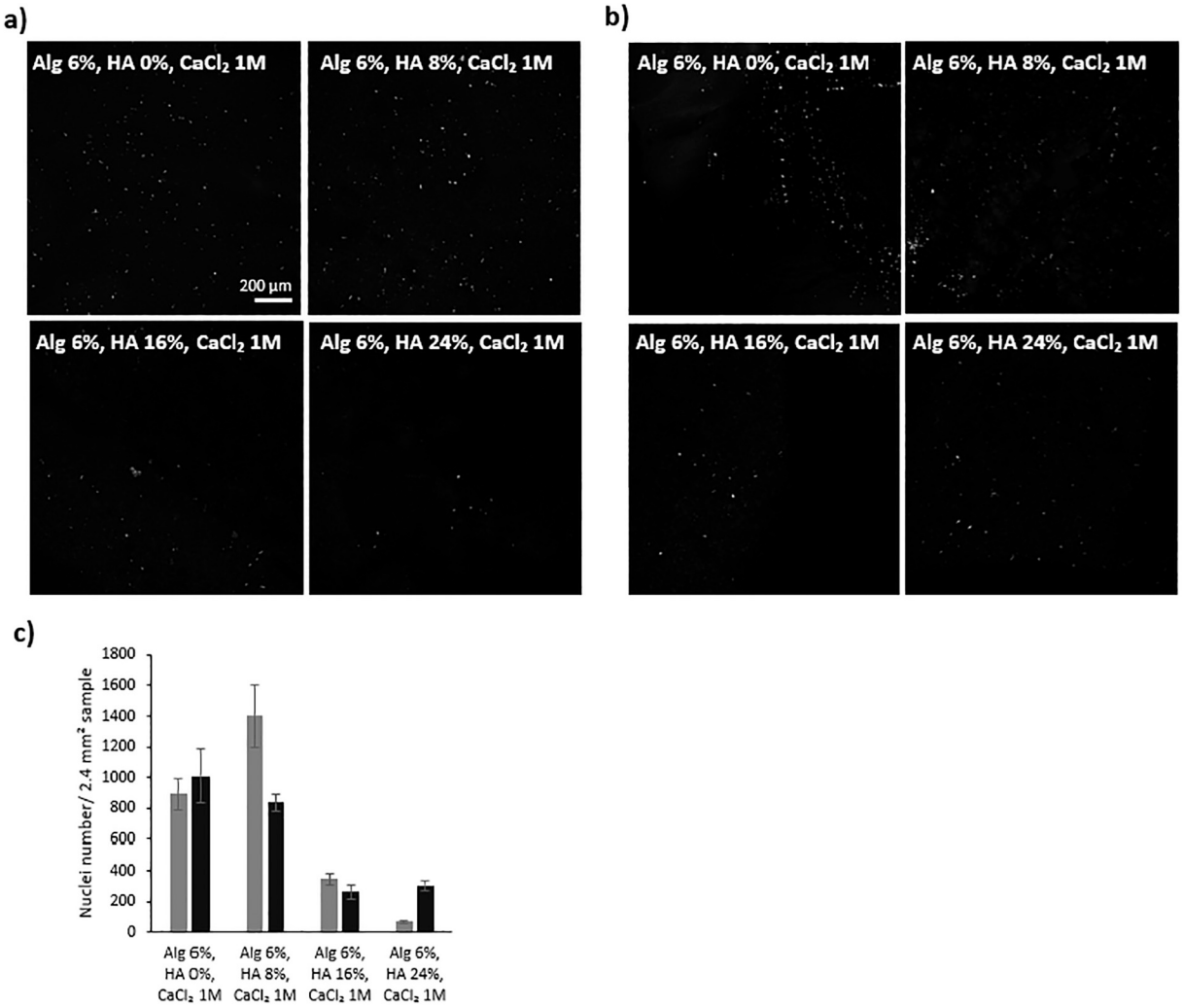

Fig. 6. Confocal microscopy images of DAPI-stained MSCs seeded on aerogel scaffolds and cultured for (a) 6, and (b) 13 days. (c) Cell attachment and proliferation tests of alginate-HA aerogels after 6 (grey bars) and 13 (black) days of culture in MSCs.

the surface area and the porosity of the materials.

No differences in MSCs attachment and spreading were observed between aerogel formulations in terms of nuclei staining (Fig. 6). The presence of HA in the scaffolds did not influence MSCs attachment as previously observed for structures with similar composition [46,49]. Nevertheless, for higher HA concentrations (16 and 24 wt%) the attachment decreases at 6 and 13 days probably due to the high superficial roughness and irregularity that generally favor cell attachment (HA concentration of 8 wt%) but at such higher levels it could make it hard for MSCs to proliferate fully attached to the aerogel.

A proliferation tendency is observed for all aerogel formulations, since more nuclei were stained after culturing scaffolds for 13 days than after 6 days (Fig. 6). This feature indicates that scaffolds were non-toxic, biocompatible, suitable for the attachment and growth of MSCs and able to promote cell adhesion and proliferation, as well as the cell colonization of the scaffold. Small pore diameters and high surface areas as obtained for the aerogels of this work are suitable for osteoblast attachment because these conditions allow cell interpenetration.

3.6. Cell migration test

Fig. 7a–f shows the evolution of the wound closure process after the scratch test with BALB cells in the presence of different aerogel formulations. Fig. 7g shows the increase in BALB cell migration in the presence of aerogel scaffolds with respect to the positive control. These are good results since the well-known bioinert properties of alginate make it hard to be degraded *in vivo* and this feature could have restricted cellular adhesion and migration as previously reported [50]. In general, structures that are stable, with satisfactory morphology and pore size allow significant human fibroblast migration in wound closure *in vitro* assays [51]. Nevertheless, finding the best microarchitecture for cell migration in tissue regeneration is still challenging. In previous studies, human dermal fibroblast migration with alginate composites showed a high closure of the scratch [51]. Furthermore, alginate composites combined with Ca^{2+} cations resulted in an enhancement on fibroblasts migration like the herein observed, probably due to changes in the regulation of genes involved in the wound healing process carried out by fibroblasts. Finally, as chemotaxis is an inherent response of cells it was hypothesized to be involved in the cell migration process since the higher concentration of biochemical factors secreted by injured tissues activate the surrounding cells and stimulate the migration of cells [52]. This biological response could also play a significant role in the increase of the migration of fibroblasts in the presence of alginate-based aerogels herein observed.

4. Conclusions

Alginate-HA aerogel scaffolds were successfully fabricated with a precise and customized nanostructure by the combination of 3D-printing and aerogel technologies. This technological combination resulted

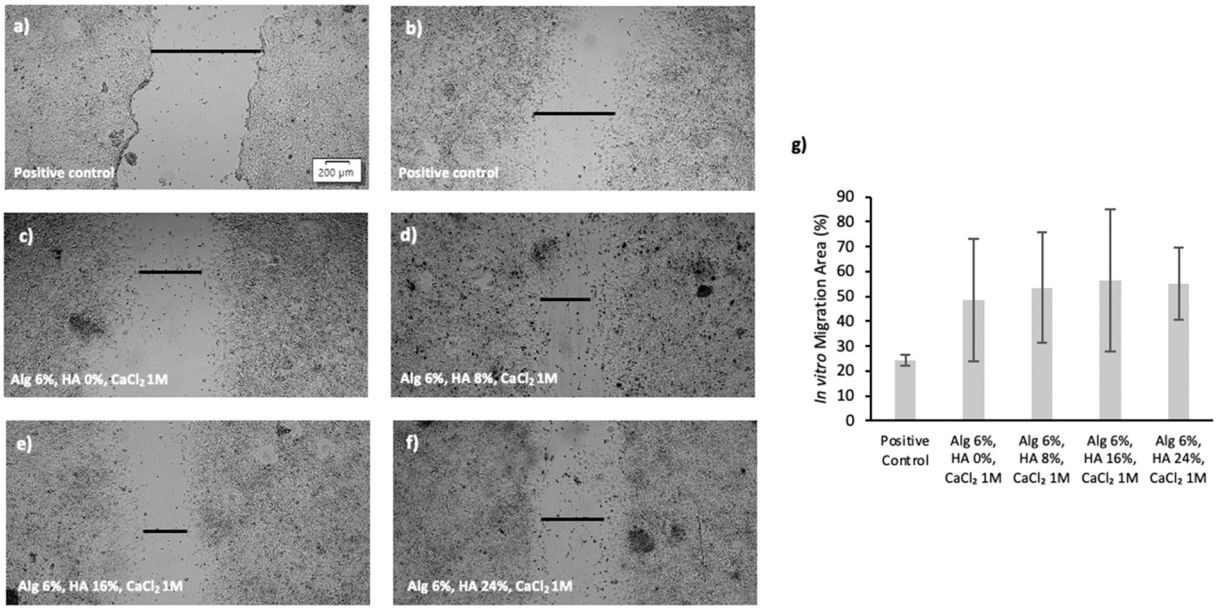

Fig. 7. Microscopy images of *in vitro* scratch test on BALB cells treated with different aerogel formulations and cultured for a) 0 h, and b–f) 24 h. g) Quantitative analysis of the stimulation of BALB cells migration by alginate-HA aerogels after 24 h in cell culture.

in nanostructured and dual porous alginate aerogels of interest for tissue engineering applications. 3D-structure is conserved after all processing steps and alginate, HA and $CaCl_2$ concentrations determine scaffold texture. An optimized scaffold formulation must provide a long-term stability and the required biocompatibility for tissue engineering applications. Cell viability tests revealed no toxicity effect or negative impact on BALB cells on normal cell environment because of the presence of the scaffold formulations. Furthermore, fibroblasts also successfully accomplished the migration process when cultured with the aerogel formulations herein proposed. MSCs were able to attach and proliferate on alginate-HA aerogels upon culture for 6 and 13 days. All these features are highly desirable for scaffolds to act as temporary supports and harbor the bone regeneration process. Finally, the fidelity of the end aerogel scaffolds with respect to the original CAD is high. Consistently, the macroporous alginate-HA aerogel scaffolds obtained by this novel technological combination of 3D-printing and supercritical drying methods represent a promising alternative for bone regenerative applications opening up new possibilities to personalized medicine. Other requirements to accomplish bone tissue formation like the degradation rate of the 3D-structures and their mechanical properties will be optimized in a future work.

Supplementary data to this article can be found online at https://doi.org/10.1016/j.msec.2021.112525.

Acknowledgments

This work was supported by Xunta de Galicia [ED431C 2020/17], MICINN [PID2020-120010RB-I00], Agencia Estatal de Investigación [AEI] and FEDER funds. Work carried out in the framework of the COST Action CA18125 “Advanced Engineering and Research of aeroGels for Environment and Life Sciences” (AERoGELS) and funded by the European Commission. A.I.-M. acknowledges to Xunta de Galicia for her predoctoral research fellowship [ED481A- 2020/104]. A. Alonso is commended for his technical contribution to this work.

Declaration of competing interest

Authors declare no conflict of interest.

References

[1] S. Yue, H. He, B. Li, T. Hou, Hydrogel as a biomaterial for bone tissue engineering: a review, Nanomaterials 10 (2020) 1511, https://doi.org/10.3390/nano10081511.
[2] N. Amiryaghoubi, M. Fathi, N.N. Pesyan, M. Samiei, J. Barar, Y. Omidi, Bioactive polymeric scaffolds for osteogenic repair and bone regenerative medicine, Med. Res. Rev. 40 (2020) 1833–1870, https://doi.org/10.1002/med.21672.
[3] Z. Wang, W. Kapadia, C. Li, F. Lin, R.F. Pereira, P.L. Granja, B. Sarmento, W. Cui, Tissue-specific engineering: 3D bioprinting in regenerative medicine, J. Control. Release 329 (2021) 237–256, https://doi.org/10.1016/j.jconrel.2020.11.044.
[4] V. Santos-Rosales, A. Iglesias-Mejuto, C.A. García-González, Solvent-Free Approaches for the Processing of Scaffolds in Regenerative Medicine 20, 2020.
[5] J.C. Boga, S.P. Miguel, D. de Melo-Diogo, A.G. Mendonça, R.O. Louro, I.J. Correia, In vitro characterization of 3D printed scaffolds aimed at bone tissue regeneration, Colloids Surf. B Biointerfaces 165 (2018) 207–218, https://doi.org/10.1016/j.colsurfb.2018.02.038.
[6] M. Askari, M. Afzali Naniz, M. Kouhi, A. Saberi, A. Zolfagharian, M. Bodaghi, Recent progress in extrusion 3D bioprinting of hydrogel biomaterials for tissue regeneration: a comprehensive review with focus on advanced fabrication techniques, Biomater. Sci. 9 (2021) 535–573, https://doi.org/10.1039/D0BM00973C.
[7] S. Naghieh, M. Sarker, N.K. Sharma, Z. Barhoumi, X. Chen, Printability of 3D printed hydrogel scaffolds: influence of hydrogel composition and printing parameters, Appl. Sci. 10 (2019) 292, https://doi.org/10.3390/app10010292.
[8] A. Dhawan, P.M. Kennedy, E.B. Rizk, I.T. Ozbolat, Three-dimensional bioprinting for bone and cartilage restoration in orthopaedic surgery, J. Am. Acad. Orthop. Surg. 27 (2019) e215–e226, https://doi.org/10.5435/JAAOS-D-17-00632.
[9] Q. Wang, Q. Xia, Y. Wu, X. Zhang, F. Wen, X. Chen, S. Zhang, B.C. Heng, Y. He, H.-W. Ouyang, 3D-printed atsttrin-incorporated Alginate/Hydroxyapatite scaffold promotes bone defect regeneration with TNF/TNFR signaling involvement, Adv. Healthc. Mater. 4 (2015) 1701–1708, https://doi.org/10.1002/adhm.201500211.
[10] C.A. García-González, T. Budtova, L. Durães, C. Erkey, P. Del Gaudio, P. Gurikov, M. Koebel, F. Liebner, M. Neagu, I. Smirnova, An opinion paper on aerogels for biomedical and environmental applications, Molecules 24 (2019) 1815, https://doi.org/10.3390/molecules24091815.
[11] G. Horvat, K. Xhanari, M. Finšgar, L. Gradišnik, U. Maver, Ž. Knez, Z. Novak, Novel ethanol-induced pectin–xanthan aerogel coatings for orthopedic applications, Carbohydr. Polym. 166 (2017) 365–376, https://doi.org/10.1016/j.carbpol.2017.03.008.
[12] V. Hegedűs, F. Kerényi, R. Boda, D. Horváth, I. Lázár, E. Tóth-Győri, B. Dezső, C. Hegedus, β-tricalcium phosphate silica aerogel as an alternative bioactive ceramic for the potential use in dentistry, Adv. Appl. Ceram. 117 (2018) 476–484, https://doi.org/10.1080/17436753.2018.1498145.
[13] M.V. Reyes-Peces, A. Pérez-Moreno, D.M. de-los-Santos, M.del M. Mesa-Díaz, G. Pinaglia-Tobaruela, J.I. Vilches-Pérez, R. Fernández-Montesinos, M. Salido, N. de la Rosa-Fox, M. Piñero, Chitosan-GPTMS-silica hybrid mesoporous aerogels for bone tissue engineering, Polymers 12 (2020) 2723, https://doi.org/10.3390/polym12112723.
[14] V. Santos-Rosales, I. Ardao, C. Alvarez-Lorenzo, N. Ribeiro, A. Oliveira, C. García-González, Sterile and dual-porous aerogels scaffolds obtained through a multistep supercritical CO2-based approach, Molecules 24 (2019) 871, https://doi.org/10.3390/molecules24050871.

[15] T. Budtova, D.A. Aguilera, S. Beluns, L. Berglund, C. Chartier, E. Espinosa, S. Gaidukovs, A. Klimek-Kopyra, A. Kmita, D. Lachowicz, F. Liebner, O. Platnieks, A. Rodríguez, L.K. Tinoco Navarro, F. Zou, S.J. Buwalda 12 (2020) 2779, https://doi.org/10.3390/polym12122779.
[16] C. Sharma, A.K. Dinda, P.D. Potdar, C.-F. Chou, N.C. Mishra, Fabrication and characterization of novel nano-biocomposite scaffold of chitosan–gelatin–alginate–hydroxyapatite for bone tissue engineering, Mater. Sci. Eng. C 64 (2016) 416–427, https://doi.org/10.1016/j.msec.2016.03.060.
[17] G. Turco, E. Marsich, F. Bellomo, S. Semeraro, I. Donati, F. Brun, M. Grandolfo, A. Accardo, S. Paoletti, Alginate/Hydroxyapatite biocomposite for bone ingrowth: a trabecular structure with high and isotropic connectivity, Biomacromolecules 10 (2009) 1575–1583, https://doi.org/10.1021/bm900154b.
[18] Y. Luo, Y. Li, X. Qin, Q. Wa, 3D printing of concentrated alginate/gelatin scaffolds with homogeneous nano apatite coating for bone tissue engineering, Mater. Des. 146 (2018) 12–19, https://doi.org/10.1016/j.matdes.2018.03.002.
[19] S. Wüst, M.E. Godla, R. Müller, S. Hofmann, Tunable hydrogel composite with two-step processing in combination with innovative hardware upgrade for cell-based three-dimensional bioprinting, Acta Biomater. 10 (2014) 630–640, https://doi.org/10.1016/j.actbio.2013.10.016.
[20] L. Ruixin, X. Cheng, L. Yingjie, L. Hao, S. Caihong, S. Weihua, A. Weining, Y. Yinghai, Q. Xiaoli, X. Yunqiang, Z. Xizheng, L. Hui, Degradation behavior and compatibility of micro, nanoHA/chitosan scaffolds with interconnected spherical macropores, Int. J. Biol. Macromol. 103 (2017) 385–394, https://doi.org/10.1016/j.ijbiomac.2017.03.175.
[21] J. Barros, M.P. Ferraz, J. Azeredo, M.H. Fernandes, P.S. Gomes, F.J. Monteiro, Alginate-nanohydroxyapatite hydrogel system: optimizing the formulation for enhanced bone regeneration, Mater. Sci. Eng. C 105 (2019), 109985, https://doi.org/10.1016/j.msec.2019.109985.
[22] M. Domingos, A. Gloria, J. Coelho, P. Bartolo, J. Ciurana, Three-dimensional printed bone scaffolds: the role of nano/micro-hydroxyapatite particles on the adhesion and differentiation of human mesenchymal stem cells, Proc. Inst. Mech. Eng. [H] 231 (2017) 555–564, https://doi.org/10.1177/0954411916680236.
[23] H. Liu, H. Peng, Y. Wu, C. Zhang, Y. Cai, G. Xu, Q. Li, X. Chen, J. Ji, Y. Zhang, H. W. OuYang, The promotion of bone regeneration by nanofibrous hydroxyapatite/chitosan scaffolds by effects on integrin-BMP/Smad signaling pathway in BMSCs, Biomaterials 34 (2013) 4404–4417, https://doi.org/10.1016/j.biomaterials.2013.02.048.
[24] X. Tang, H. Zhou, Z. Cai, D. Cheng, P. He, P. Xie, D. Zhang, T. Fan, Generalized 3D printing of graphene-based mixed-dimensional hybrid aerogels, ACS Nano 12 (2018) 3502–3511, https://doi.org/10.1021/acsnano.8b00304.
[25] Junzong Feng, B.-L. Su, H. Xia, S. Zhao, C. Gao, L. Wang, O. Ogbeide, Jian Feng, T. Hasan, Printed aerogels: chemistry, processing, and applications, Chem. Soc. Rev. 50 (2021) 3842–3888, https://doi.org/10.1039/C9CS00757A.
[26] H. Maleki, T. Fischer, C. Bohr, J. Auer, S. Mathur, B. Milow, Hierarchically organized biomimetic architectured silk Fibroin–Ceramic-based anisotropic hybrid aerogels for thermal energy management, Biomacromolecules 22 (2021) 1739–1751, https://doi.org/10.1021/acs.biomac.1c00175.
[27] H. Maleki, S. Montes, N. Hayati-Roodbari, F. Putz, N. Huesing, Compressible, thermally insulating, and fire retardant aerogels through self-assembling silk fibroin biopolymers inside a silica structure—an approach towards 3D printing of aerogels, ACS Appl. Mater. Interfaces 10 (2018) 22718–22730, https://doi.org/10.1021/acsami.8b05856.
[28] V. Santos-Rosales, G. Alvarez-Rivera, M. Hillgärtner, A. Cifuentes, M. Itskov, C. A. García-González, A. Rege, Stability studies of starch aerogel formulations for biomedical applications, Biomacromolecules 21 (2020) 5336–5344, https://doi.org/10.1021/acs.biomac.0c01414.
[29] H. Tetik, D. Feng, S.W. Oxandale, G. Yang, K. Zhao, K. Feist, N. Shah, Y. Liao, Z. C. Leseman, D. Lin, Bioinspired manufacturing of aerogels with precisely manipulated surface microstructure through controlled local temperature gradients, ACS Appl. Mater. Interfaces 13 (2021) 924–931, https://doi.org/10.1021/acsami.0c19087.
[30] Ö.E. Akdere, İ. Shikhaliyeva, M. Gümüşderelioğlu, Boron mediated 2D and 3D cultures of adipose derived mesenchymal stem cells, Cytotechnology 71 (2019) 611–622, https://doi.org/10.1007/s10616-019-00310-9.
[31] C.A. García-González, J. Barros, A. Rey-Rico, P. Redondo, J.L. Gómez-Amoza, A. Concheiro, C. Alvarez-Lorenzo, F.J. Monteiro, Antimicrobial properties and osteogenicity of vancomycin-loaded synthetic scaffolds obtained by supercritical foaming, ACS Appl. Mater. Interfaces 10 (2018) 3349–3360, https://doi.org/10.1021/acsami.7b17375.
[32] Z. Sartawi, K.B. Ryan, C. Waeber, Bone regenerative potential of the selective sphingosine 1-phosphate receptor modulator siponimod: in vitro characterisation using osteoblast and endothelial cells, Eur. J. Pharmacol. 882 (2020), 173262, https://doi.org/10.1016/j.ejphar.2020.173262.
[33] J. Zhang, X. Liu, H. Li, C. Chen, B. Hu, X. Niu, Q. Li, B. Zhao, Z. Xie, Y. Wang, Exosomes/tricalcium phosphate combination scaffolds can enhance bone regeneration by activating the PI3K/Akt signaling pathway, Stem Cell Res Ther 7 (2016) 136, https://doi.org/10.1186/s13287-016-0391-3.
[34] M.P. Batista, V.S.S. Gonçalves, F.B. Gaspar, I.D. Nogueira, A.A. Matias, P. Gurikov, Novel alginate-chitosan aerogel fibres for potential wound healing applications, Int. J. Biol. Macromol. 156 (2020) 773–782, https://doi.org/10.1016/j.ijbiomac.2020.04.089.
[35] S. Naghieh, M.R. Karamooz-Ravari, M. Sarker, E. Karki, X. Chen, Influence of crosslinking on the mechanical behavior of 3D printed alginate scaffolds: experimental and numerical approaches, J. Mech. Behav. Biomed. Mater. 80 (2018) 111–118, https://doi.org/10.1016/j.jmbbm.2018.01.034.
[36] K. Chen, H. Zhang, Alginate/pectin aerogel microspheres for controlled release of proanthocyanidins, Int. J. Biol. Macromol. 136 (2019) 936–943, https://doi.org/10.1016/j.ijbiomac.2019.06.138.
[37] M.D. Giuseppe, N. Law, B. Webb, R. A. Macrae, L.J. Liew, T.B. Sercombe, R. J. Dilley, B.J. Doyle, Mechanical behaviour of alginate-gelatin hydrogels for 3D bioprinting, J. Mech. Behav. Biomed. Mater. 79 (2018) 150–157, https://doi.org/10.1016/j.jmbbm.2017.12.018.
[38] H.-R. Lin, Y.-J. Yeh, Porous alginate/hydroxyapatite composite scaffolds for bone tissue engineering: preparation, characterization, andin vitro studies, J. Biomed. Mater. Res. 71B (2004) 52–65, https://doi.org/10.1002/jbm.b.30065.
[39] J. Sun, H. Tan, Alginate-based biomaterials for regenerative medicine applications, Materials 6 (2013) 1285–1309, https://doi.org/10.3390/ma6041285.
[40] H.-W. Kim, J.C. Knowles, H.-E. Kim, Hydroxyapatite and gelatin composite foams processed via novel freeze-drying and crosslinking for use as temporary hard tissue scaffolds, J. Biomed. Mater. Res. A 72A (2005) 136–145, https://doi.org/10.1002/jbm.a.30168.
[41] M. Alnaief, R.M. Obaidat, M.M. Alsmadi, Preparation of hybrid alginate-chitosan aerogel as potential carriers for pulmonary drug delivery, Polymers 12 (2020) 2223, https://doi.org/10.3390/polym12102223.
[42] T. Athamneh, A. Amin, E. Benke, R. Ambrus, P. Gurikov, I. Smirnova, C.S. Leopold, Pulmonary drug delivery with aerogels: engineering of alginate and alginate-hyaluronic acid microspheres, Pharm. Dev. Technol. 26 (2021) 509–521, https://doi.org/10.1080/10837450.2021.1888979.
[43] R. Subrahmanyam, P. Gurikov, I. Meissner, I. Smirnova, Preparation of biopolymer aerogels using green solvents, J. Vis. Exp. 54116 (2016), https://doi.org/10.3791/54116.
[44] A. Veronovski, Z. Novak, Ž. Knez, Synthesis and use of organic biodegradable aerogels as drug carriers, J. Biomater. Sci. Polym. Ed. 23 (2012) 873–886, https://doi.org/10.1163/092050611X566126.
[45] P. Panraksa, S. Udomsom, P. Rachtanapun, C. Chittasupho, W. Ruksiriwanich, P. Jantrawut, Hydroxypropyl methylcellulose E15: a hydrophilic polymer for fabrication of orodispersible film using syringe extrusion 3D printer, Polymers 12 (2020) 2666, https://doi.org/10.3390/polym12112666.
[46] N.A. Kamalaldin, B.H. Yahya, A. Nurazreena, Cell evaluation on Alginate/Hydroxyapatite block for biomedical application, Procedia Chem. 19 (2016) 297–303, https://doi.org/10.1016/j.proche.2016.03.012.
[47] Th.I. Shaheen, A.S. Montaser, S. Li, Effect of cellulose nanocrystals on scaffolds comprising chitosan, alginate and hydroxyapatite for bone tissue engineering, Int. J. Biol. Macromol. 121 (2019) 814–821, https://doi.org/10.1016/j.ijbiomac.2018.10.081.
[48] K.M. Tohamy, M. Mabrouk, I.E. Soliman, H.H. Beherei, M.A. Aboelnasr, Novel alginate/hydroxyethyl cellulose/hydroxyapatite composite scaffold for bone regeneration: in vitro cell viability and proliferation of human mesenchymal stem cells, Int. J. Biol. Macromol. 112 (2018) 448–460, https://doi.org/10.1016/j.ijbiomac.2018.01.181.
[49] L. Benning, L. Gutzweiler, K. Tröndle, J. Riba, R. Zengerle, P. Koltay, S. Zimmermann, G.B. Stark, G. Finkenzeller, Cytocompatibility testing of hydrogels toward bioprinting of mesenchymal stem cells: cytocompatibility testing of hydrogels, J. Biomed. Mater. Res. A 105 (2017) 3231–3241, https://doi.org/10.1002/jbm.a.36179.
[50] B. Yao, T. Hu, X. Cui, W. Song, X. Fu, S. Huang, Enzymatically degradable alginate/gelatin bioink promotes cellular behavior and degradation in vitro and in vivo, Biofabrication 11 (2019), 045020, https://doi.org/10.1088/1758-5090/ab38ef.
[51] R. Gallardo-Rivera, M. de los Ángeles Aguilar-Santamaría, P. Silva-Bermúdez, J. García-López, A. Tecante, C. Velasquillo, A. Román-Guerrero, C. Pérez-Alonso, H. Vázquez-Torres, K. Shirai, Polyelectrolyte complex of Aloe vera, chitosan, and alginate produced fibroblast and lymphocyte viabilities and migration, Carbohydr. Polym. 192 (2018) 84–94, https://doi.org/10.1016/j.carbpol.2018.03.044.
[52] C. Lin, B. Tao, Y. Deng, Y. He, X. Shen, R. Wang, L. Lu, Z. Peng, Z. Xia, K. Cai, Matrix promote mesenchymal stromal cell migration with improved deformation via nuclear stiffness decrease, Biomaterials 217 (2019), 119300, https://doi.org/10.1016/j.biomaterials.2019.119300.
[53] A. Salerno, C. Domingo, Making microporous nanometre-scale fibrous PLA aerogels with clean and reliable supercritical CO2 based approaches, Microporous Mesoporous Mater. 184 (2014) 162–168, https://doi.org/10.1016/j.micromeso.2013.10.019.
[54] C.A. García-González, A. Concheiro, C. Alvarez-Lorenzo, Processing of Materials for Regenerative Medicine Using Supercritical Fluid Technology, Bioconjug. Chem. 26 (2015) 1159–1171, https://doi.org/10.1021/bc5005922.
[55] M. Martins, A.A. Barros, S. Quraishi, P. Gurikov, S.P. Raman, I. Smirnova, A.R. C. Duarte, R.L. Reis, Preparation of macroporous alginate-based aerogels for biomedical applications, J. Supercrit. Fluids 106 (2015) 152–159, https://doi.org/10.1016/j.supflu.2015.05.010.